GDCh Research Article Angewandte International Edition Chemie www.angewandte.org

How to cite: *Angew. Chem. Int. Ed.* **2024**, *63*, e202402973
doi.org/10.1002/anie.202402973

Inorganic Materials

Translocation and Confinement of Tetraamines in Adaptable Microporous Cavities

*Ana Rubio-Gaspar[+], Alechania Misturini[+], Reisel Millan, Neyvis Almora-Barrios, Sergio Tatay, Volodymyr Bon, Mickaele Bonneau, Vincent Guillerm, Mohamed Eddaoudi, Sergio Navalón, Stefan Kaskel, Donatella Armentano, and Carlos Martí-Gastaldo**

Abstract: Metal-Organic Frameworks can be grafted with amines by coordination to metal vacancies to create amine-appended solid adsorbents, which are being considered as an alternative to using aqueous amine solutions for CO_2 capture. In this study, we propose an alternative mechanism that does not rely on the use of neutral metal vacancies as binding sites but is enabled by the structural adaptability of heterobimetallic Ti_2Ca_2 clusters. The combination of hard (Ti^{4+}) and soft (Ca^{2+}) metal centers in the inorganic nodes of the framework enables MUV-10 to adapt its pore windows to the presence of triethylenetetramine molecules. This dynamic cluster response facilitates the translocation and binding of tetraamine inside the microporous cavities to enable the formation of bis-coordinate adducts that are stable in water. The extension of this grafting concept from MUV-10 to larger cavities not restrictive to CO_2 diffusion will complement other strategies available for the design of molecular sorbents for decarbonization applications.

Introduction

The field of Reticular Chemistry has in the quasi-arithmetic design of porous architectures one of its main strengths. Both, Metal-Organic Frameworks (MOFs) and Covalent-Organic Frameworks (COFs) share equivalent geometrical concepts in their design, although adapted to the particularities of the use of coordination or covalent bonds as structural linkages, and metal clusters or organic molecules as structure-directing units.[1–3] This conceptual basis has made it possible to produce an enormous number of molecular frameworks in which the regular organization in space of compositionally versatile molecular units provides control over the chemistry[4] or metrics[5] of their porosity. These features often dictate guest recognition, mass transfer and volumetric adsorption capacity, all central to their application in gas storage,[6–8] separation[9–13] or catalysis.[14–17]

Although many of the applications of these materials are based on the intrinsic properties of a given framework, it is true that the periodic distribution of molecular units and pores also provides an ideal canvas for incorporating additional molecular components that inherit the order imposed by the templating net and can be used to modify its properties or introduce new functionalities. This can be done by the covalent linkage of molecules to reactive tags in the organic linker by post-synthetic modification (PSM)[18] or by coordinative grafting to open vacant sites in the metal nodes,[19–21] adequate to achieve a regular arrangement of the newly incorporated organic units.

Although these approaches have been generally applied for the incorporation of organic and inorganic components, and in a broad range of applications, in recent years, the interest on the incorporation of alkyl amines to MOFs has been intensified due to the strong affinities of amines for

[*] A. Rubio-Gaspar,[+] Dr. A. Misturini,[+] Dr. N. Almora-Barrios, Prof. S. Tatay, Prof. C. Martí-Gastaldo
Functional Inorganic Materials Team, Instituto de Ciencia Molecular (ICMol), Universidad de València,
c/Catedrático José Beltrán, 2. Paterna 46980, Spain
E-mail: carlos.marti@uv.es

Dr. R. Millan
Instituto de Tecnología Química (ITQ), Universitat Politècnica de València-Consejo Superior de Investigaciones Científicas (CSIC), Valencia 46022, Spain

Dr. V. Bon, Prof. S. Kaskel
Technische Universität Dresden, Department of Inorganic Chemistry
Dresden 01069, Germany

Dr. M. Bonneau, Dr. V. Guillerm, Prof. M. Eddaoudi
Functional Materials Design, Discovery and Development Research Group, Advanced Membranes and Porous Materials Center, Division of Physical Sciences and Engineering,
King Abdullah University of Science and Technology,
Thuwal, Saudi Arabia

Prof. S. Navalón
Departamento de Química,
Universitat Politècnica de València,
Valencia 46022, Spain

Prof. D. Armentano
Dipartimento di Chimica e Tecnologie Chimiche (CTC),
Università della Calabria,
87036 Rende, Cosenza, Italy

[+] These authors contributed to the work equally.

carbon dioxide, which can result in solid sorbents with the capacity to capture it directly from the air (DAC).[22–24] This alternative to the use of aqueous amine solutions can also overcome some of its limitations, such as thermal degradation, oxidative stress or low CO_2 working capacities.[25,26] To date, the generation of amine-appended frameworks has been dominated by their grafting to the neutral coordination vacancies that are generated by vacuum heat treatment of two primary types of secondary building units (SBUs). These include the $[Cr_3(\mu_3\text{-}O)(X)(RCO_2)_3(H_2O)_2]$ ($X = F^-$, OH^-) trimers in MIL-101,[27] triazole and $[M_2(RCO_2)(H_2O)_2]$ ($M = Mg^{2+}$, Zn^{2+}) rod-shape chains in MOF-74-type frameworks (Figure 1a).[22–24,28–34] In addition, both families display fairly high porosity with pore volumes and windows big enough to facilitate amine diffusion and grafting. However, single crystal structural studies are only available for MOF-74 derivatives, also referred to as CPO-27.[35] As beautifully illustrated by Long's group for the case of diamines and tetraamines, their size and denticity can determine different incorporation patterns depending on their relative variation with respect to the distances between adjacent metal vacancies across a single chain or the distance separating neighboring chains, a parameter that is fixed by the hexagonal channels of Mg_2(dobpdc), related to MOF-74 (Figure 1a).[23,30] These differences are not simply structural but can result into greater thermal and hydrolytic stability of the amino-appended sorbent, suggesting that beyond the presence of the amine, the way it is coordinated to different porous scaffolds may be even more important in determining the properties of the final material.[36]

We recently described the possibility of generating thermal vacancies in the heterobimetallic cluster Ti_2Ca_2 amenable to the synthesis of isoreticular titanium frameworks,[37,38] as an anchor point for the selective grafting of 1,3-diaminopropane (DAP) molecules to Ca^{2+} sites.[39] Inspired by the differences observed between tetraamines of variable length for the case of Mg_2(dobpdc),[30] we decided to investigate whether these changes in the coordination pattern induced by the size and denticity of the amine could also be extended to the MUV-10 **the**net, characterized by the presence of a three-dimensional porosity with smaller pore windows and distances between neighboring grafting sites (Figure 1b, d_{inter}) arguably more adequate to induce bridging coordination modes across the accessible pores for superior stability. To our surprise, our results reveal a new mechanism for the translocation of tetraamines into the microporous cavities of MUV-10 as most favourable anchorage sites. The presence of soft coordination bonds in the framework enables the reversible reconfiguration of the pore windows, that facilitate the caging of the amine form the formation of bis-coordinated chelates that are insensitive to moisture. This method of integrating amines is intimately linked to the structural flexibility intrinsic to MOFs and illustrates the opportunities that porous molecular frameworks can offer for the development of amine-appended adsorbents not accessible to more rigid hosts.

Results and Discussion

Coordinative Grafting of Tetraamines in MUV-10

As shown in Figure 1b, the cubic structure of $[Ti_2Ca_2(\mu_3\text{-}O)_2(btc)_{2.67}(H_2O)_4]$ features 3D intersected channels resulting in the formation of cuboctahedral and octahedral cavities (pink and beige spheres in Figure 1b) with similar internal diameters of near to 1.0 and 0.8 nm. Each cluster shows a regular distribution of coordinated water molecules in the axial positions of Ti^{4+} and Ca^{2+} sites. Like in $[Mg_2(dobpdc)(H_2O)_2]$, these axial water molecules can be removed by vacuum heat treatment to generate coordination vacancies as demonstrated previously by water adsorption isotherms and FT-IR spectroscopy of adsorbed CO.[39] The main difference in our case using MUV-10 solid is the presence of smaller pore openings of approximately 0.5 nm in diameter, compared to more than 1.5 nm in Mg_2(dobpdc). Accord-

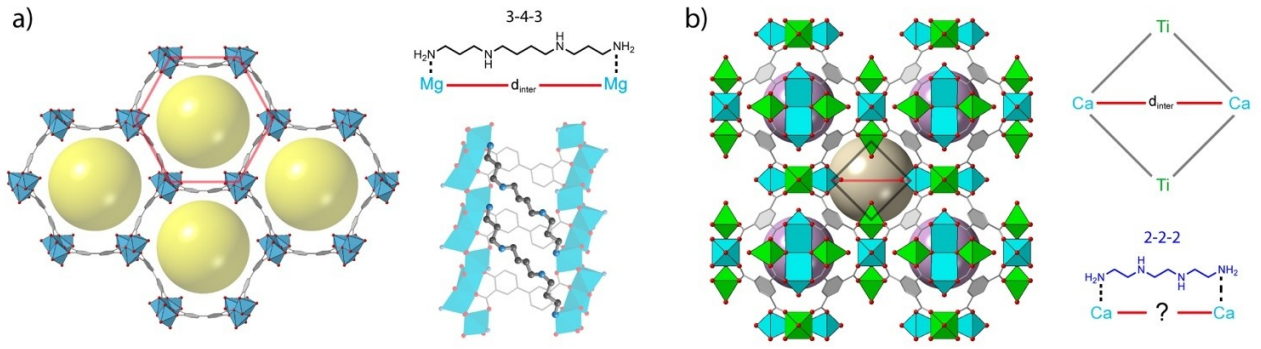

Figure 1. Extension of the concept of tetraamine coordination in molecular networks to other periodic distributions of coordination vacancies. a) Structure of Mg_2(dobpdc) (dobpdc = 4,4'-dioxidobiphenyl-3,3'-dicarboxylate) showing the distribution of Mg-oxo chains in its hexagonal channels (*left*). The flexibility and size of the tetraamine *N,N'*-(butane-1,4-diyl)bis(propane-1,3-diamine) (3-4-3) allows it to coordinate two Mg^{2+} sites in neighboring chains for the formation of more stable adducts (*right*). b) Structure of MUV-10 showing the cubic distribution of Ti_2Ca_2 clusters and their relative spacing along the channels that form a three-dimensional network (*left*). For this study, we chose triethylenetetramine (2-2-2 or TETA) with a size well suited to chelate two Ca^{2+} sites separated near to 12 Å in the cuboctahedral cavities along the channel.

ingly, we chose to use triethylenetetramine (2-2-2 or TETA), which in addition to being the smallest tetraamine available, can also bridge opposite Ca^{2+} sites in the channels separated by near 1.2 nm. According to the protocol established by Long and co-workers, once the desolvated crystals were prepared, a concentrated solution of TETA in anhydrous toluene (0.3 M) was added to the crystals under an inert atmosphere, and the mixture was left to react at room temperature for 12 hours. Next, the amine-appended crystals were washed with anhydrous toluene and hexane to remove any excess of uncoordinated TETA and dried at 120 °C under vacuum for 6 hours. The presence of tetraamines in the solid was first qualitatively confirmed with FT-IR spectroscopy (Supplementary Section S5.2). As for the crystallinity of the sample, powder X-ray diffraction (PXRD) confirmed a negligible impact on the crystallinity of the material after the modification. To quantify the amount of amine incorporated, the MUV-10-TETA crystals were digested in basic media and analysed with ^{1}H NMR to confirm the presence of approximately 1 TETA molecule per Ti_2Ca_2 cluster.

At this point, it is important to note that although the methodology used to incorporate TETA into MUV-10 is the same used for the case of the diamine DAP,[39] we always observed a better response of the crystals to TETA incorporation in terms of structure stability and changes in crystal morphology after grafting (Figures 2a and 2b). In the case of MUV-10-DAP, our efforts to analyze the diamine coordination by single crystal X-ray diffraction remained unsuccessful and we were forced to use indirect characterization methods. In turn, the MUV-10-TETA crystals not only maintained the octahedral morphology of the pristine MOF but also exhibited diffraction at resolutions of near 1 Å, that also features a diffuse scattering pattern suggesting the presence of correlated structural disorder in the framework (Figure 2c).[40] This encouraged us to collect high-quality diffraction data at I19 beamline at Diamond Light Source (ID CY28808-1). The single crystal structure of MUV-10-TETA confirms the preference of the tetraamine binding Ca^{2+} sites in the Ti_2Ca_2 cluster. As shown in Figure 2d and 2e, the coordination geometry of calcium (II) changes from capped trigonal prismatic 7-coordinated (7-c) to tricapped trigonal prismatic (9-c) as result of the coordination of two TETA molecules with Ca–N bonds of 2.24 Å, compared to the O-donor carboxylates that display Ca–O distances of 2.34 Å. Compared to the DAP case, the tetraamine does not get accommodated inside the more accessible cuboctahedral cavities along the channels of MUV-10, but it is instead trapped inside the smaller octahedral cavities. This is quite surprising since, although both cavities are relatively similar in size, with crystallographic pore diameters of 1.0 and 0.8 nm, the translocation of TETA from the 3D channels into these cavities shall be disfavored by the comparatively smaller pore windows and corresponding difficulties for the diffusion of the amine. TETA molecules inside the cavities present a pronounced crystallographic disorder that does not respect the intrinsic *Pm-3* cubic symmetry of the framework (Figure 2f). This positional disorder is probably responsible for the diffuse scattering mentioned above. The refined structural model accounts for the presence of 3 TETA molecules per octahedral cage, which share the same conformation but are overlapped between 12 positions around the (0,0,0) point symmetry element (Figure 2g) for an overall formula of $[Ti_2Ca_2(\mu_3\text{-}O)_2(btc)_{2.67}]\cdot$TETA. The tetraamines adopt the most adequate conformation to bridge two Ca^{2+} sites separated 10.10(1) Å along the edges defined by the octahedral cavity (Figure 2h). These sites belong to neighboring Ti_2Ca_2 clusters located at the vertices of the octahedral cavity, thus confirming the ability of TETA to form bridging coordination modes reminiscent of those encountered in Mg_2(dobpdc)-3-3-3.[30] According to the crystallographic content per unit formula $[Ti_2Ca_2(\mu_3\text{-}O)_2(btc)_{2.67}(H_2O)_4(TETA)_{0.75}]$, this would statistically correspond to the simultaneous occupation of at least 3 of the 12 edges of the octahedron by bridging TETA molecules.

Binding of Tetraamine and Translocation Mechanism

As already discussed, the formation of a TETA complex within the octahedral boxes of MUV-10 was far from our original expectations. Because our previous work showed that the diamine DAP only coordinates a single Ca^{2+} site per molecule and is presumably localized into the more accessible channels of the framework,[39] we turned to computational tools to better understand the grafting mechanism after using thermogravimetric analysis to discard the presence of missing linker defects that might facilitate diffusion (Figure S10). Specifically, we aimed to elucidate the mechanism that controls the translocation of TETA from the channels into the octahedral cavities and rationalize why the comparatively smaller DAP behaves differently.

For the latter, we employed periodic DFT calculations with the VASP code by using the experimental structure of MUV-10-TETA as starting point. This was modified with Materials Studio R7 to account for the presence of TETA or DAP in different molecular geometries for identifying the most energetically favorable binding mode in each case. Methodological details are summarized in Section S.4.1 of the Supporting Information. Our calculations show that the conformational flexibility of TETA, as result of its longer alkyl chains, enables a conformation compatible with the coordination by the same TETA molecule of two Ca^{2+} sites from adjacent clusters (Figure 3b). This coordination mode is almost identical to that obtained experimentally, although the Ca–N distances are elongated to 2.9 Å, likely due to the use of only one amine molecule per cavity in our simulations. In the DAP case, the rigidity imposed by a shorter chain restricts its conformation to the coordination of a single metal center (Figure 3a). From an energetic point of view, this translates into a much more robust grafting for the case of tetraamine, which forms an adduct 53 kJ mol^{-1} more stable than that accessible to the diamine.

Regarding the tetraamine diffusion, we used the Umbrella Sampling (US) method to calculate the free energy profile along a selected coordinate that unambiguously

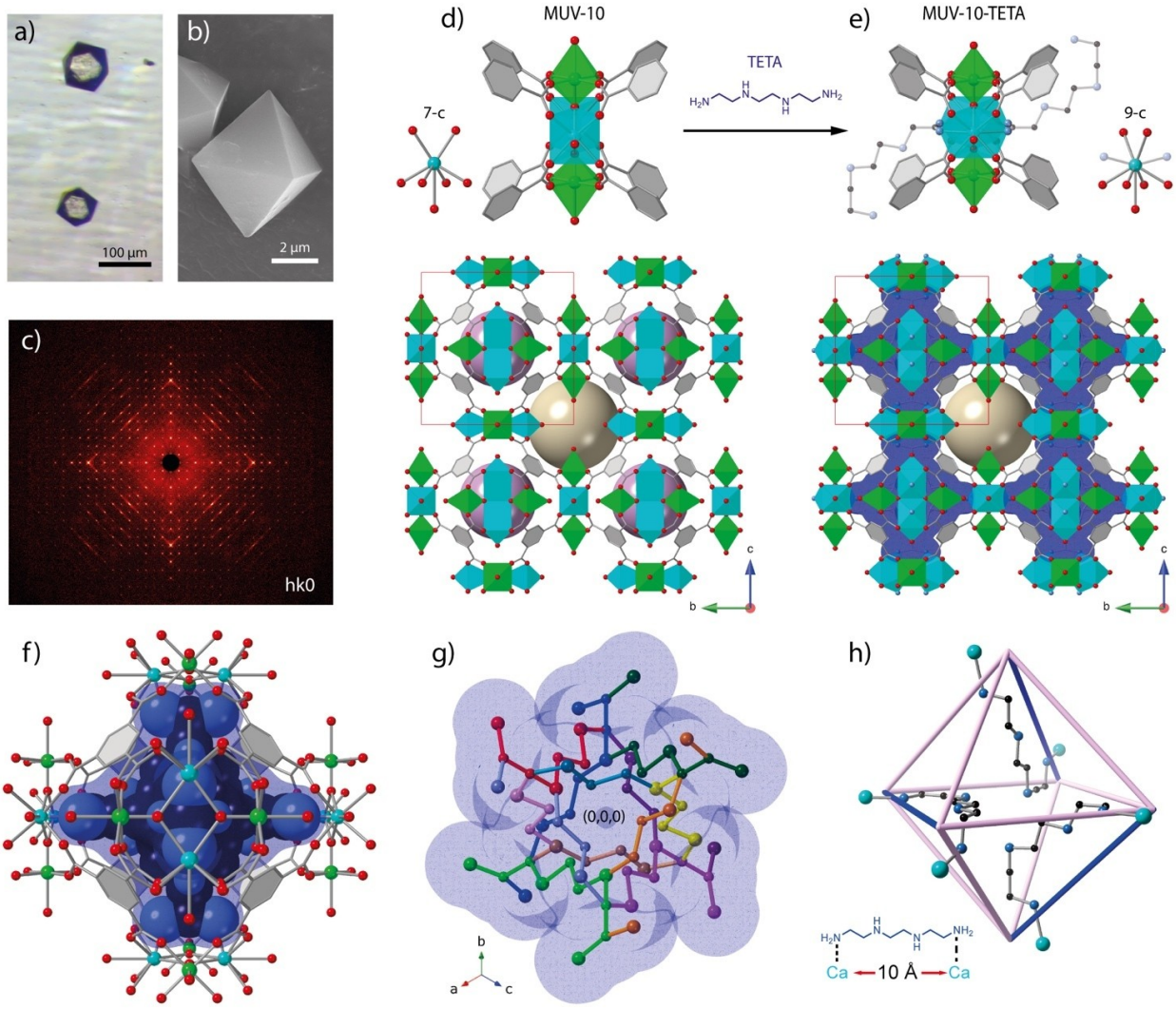

Figure 2. Coordinative grafting of tetraamines in MUV-10. a, b) MUV-10-TETA crystals viewed with optical and scanning electron microscopy. Note that the images correspond to different batches used for single crystal studies (*left*) and additional characterization (*right*). Please check Supplementary Section S.2 for experimental details. c) Diffraction image showing the presence of oriented diffuse scattering patterns on hk0 at 0.8 Å resolution indicative of structural disorder. d, e) Impact of TETA coordination on the structure of MUV-10. *Top*: Changes in the coordination sphere of Ca^{2+} sites (pale blue) that evolve from 7-connected to 9-c as result of the grafting of the tetraamine. Ti^{4+} sites are represented in green. Some carbon atoms in the amine backbone were refined as coplanar. Although this is unrealistic, it is the best model we could refine due to the cavity size and the underlying disorder. *Bottom*: view of the framework along the *z* axis showing the occupation of the octahedral cavities (magenta spheres) with disordered TETA molecules represented by their Van der Waals surface (blue). The cubooctahedral cavities (salmon spheres) along the intersected channels in the framework remain accessible also in MUV-10-TETA. f) Zoom of the octahedral cavities showing the structural disorder of the TETA molecules inside, represented by their thermal ellipsoids. g) The cavity can accommodate 12 crystallographically equivalent conformations related by symmetry. Each one of them is represented with a different colour. h) Simplification of the octahedral cage showing the coordination mode adopted by TETA to bridge intercluster Ca^{2+} sites located at the vertices and separated by close to 10 Å. The crystallographic content accounts for the simultaneous grafting of 3 tetraamines that would be accommodated in the corresponding number of edges. Occupied edges are highlighted in blue.

represents this process.[41] Inspired by previous studies with zeolites,[42–44] we used the collective variable ξ to track the diffusion of TETA molecules at 300 K across the pore windows that grant access to the octahedral cavities in MUV-10 (Figure 3c). Considering the average plane that contains the ring (in grey), ξ values represent the projection (dark blue arrow) of the TETA position vector (light blue arrow, that considers the geometric centre of the three atoms highlighted in light blue) on the vector normal to the plane (grey arrow). The collective variable is zero when TETA projection lies on the ring plane, taking negative or positive values once inside or outside the cavity, respectively. Further computational details are summarized in Section S.4.3 of the Supporting Information.

TETA translocation would involve diffusion through any of the 12 pore windows available in the cavity (Figure 3d).

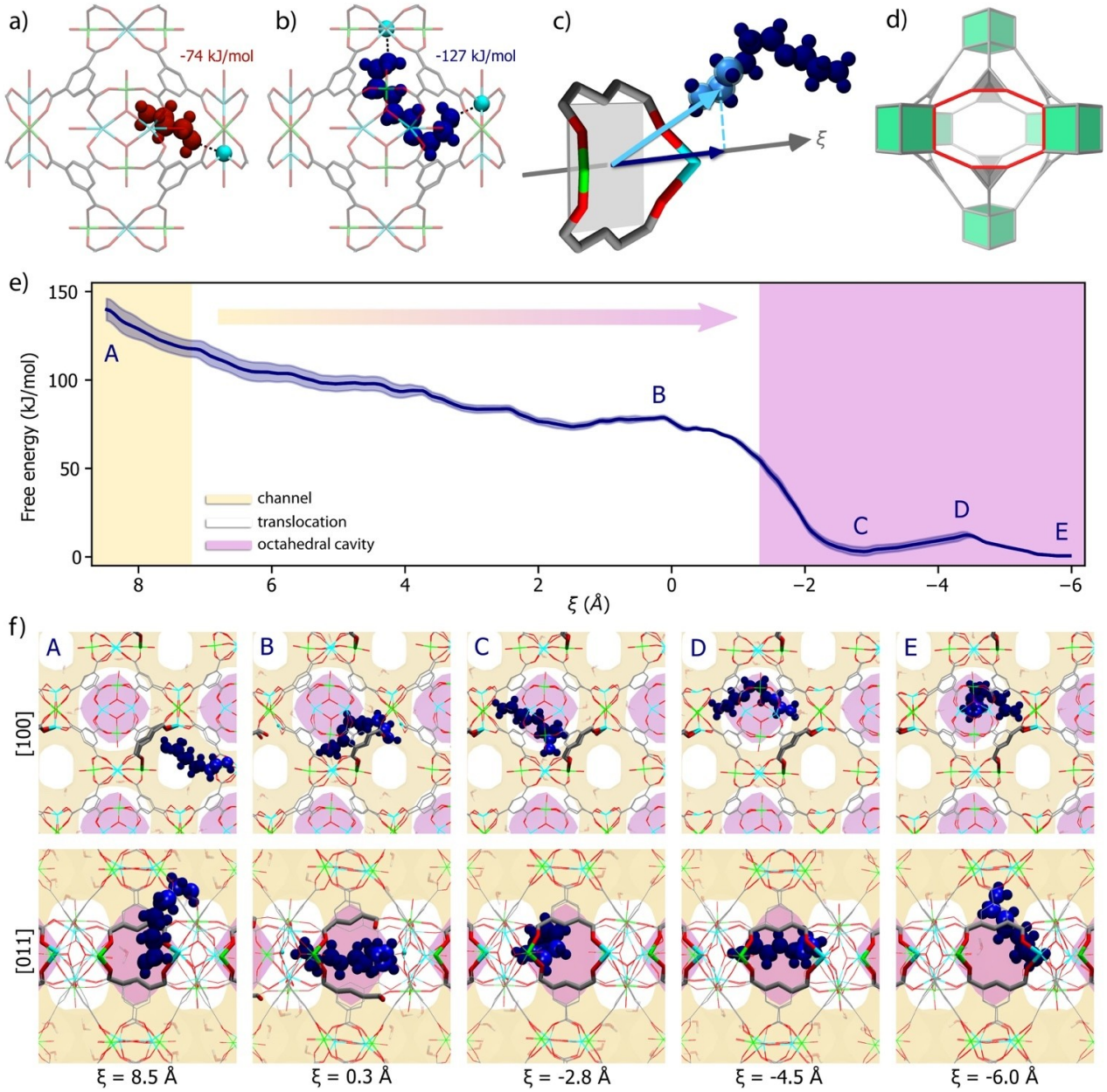

Figure 3. Binding of tetraamine and translocation mechanism. a, b) Adsorption energy of DAP (red) and TETA (blue) molecules inside MUV-10 cage, with distances Ca–N in black. c) Schematic representation of the collective variable (ξ) that describes TETA diffusion through MUV-10 pore opening. d) Perspective of the pore aperture along the [111] axis highlighted in red. e) Average Helmholtz free energy profile for TETA translocation process considering three replicate simulations for every ξ value, and standard error of the mean with transparency. f) Snapshots of amine conformations along [100] and [011] axes throughout TETA diffusion. Pink and yellow regions in e) and f) correspond to MUV-10 octahedral cage and 3D channel system, respectively. Hydrogen atoms from Ti axial waters and aromatic rings were omitted.

However, our geometrical analysis of host and guest structures reveal that even by adopting an unfolded conformation, the size of the windows is apparently too narrow to allow the passage of the tetraamine (Supporting Information Section S.4.2). Nevertheless, the Helmholtz free energy profile represented in Figure 3e confirms that the translocation of TETA from the channel (state A) into the cavity (states C to E) is a nearly barrierless process with a significant decrease in the free energy of the system of ~140 kJ mol^{-1}. In other words, although the translocation of TETA is thermodynamically favorable, the process will necessarily involve the unfolding of TETA and a reconfiguration of the windows that give access to the cavity for a wider opening in presence of the guest molecule.

All these features are captured by our US simulations. The tetraamine adopts its most folded conformations inside the channels (ξ = 8 to 7 Å, yellow region in Figure 3e), which are characterized by the average intramolecular N···N distance between terminal -NH_2 groups of around 5–6 Å. However, it unfolds upon crossing the window (white region

in Figure 3e) to adopt an elongated conformation with longer intramolecular distance of up to 9.5 Å at the earliest stage (ξ = 7 to 4 Å), that helps minimizing the guest limiting molecular dimension to facilitate its infiltration as anticipated by our geometrical analysis (Section S.4.2). This conformational change of TETA also triggers a dynamic response of the pore window, which was studied with the GFN-FF model due to its improved description of bonded and nonbonded interactions compared to most common classical force fields. The diffusion process (ξ = 7 to −1 Å) is also associated to the sequential breaking of two of the four coordination bonds of the softer Ca^{2+} sites with the bridging carboxylate groups in the Ti_2Ca_2 cluster, that widens the window to enable TETA to go through (state B in Figure 3f). The window reconfiguration and reorientation of the detached carboxylate groups enables the formation of a network of additional H-bonds that stabilize its opening. A complementary discussion on this can be found in the Supplementary Section S.4.3.3. In turn, the harder Ti^{4+} sites can accommodate this structural distortion with minimum deviations of 0.1 Å in the Ti–O bond lengths compared to the crystallographic value (2.03 Å), for all simulations analysed. Once the process of translocation is completed, the Ca–O bonds are re-established and the local deformations in the window and cluster involved are recovered. This dynamic bonding mode is consistent with variable temperature diffuse reflectance spectroscopy (VT-DRIFTS) measurements by Brozek and co-workers that support the labile nature of Ca–O bonds in MUV-10(Ca).[45,46] Once inside the cavity, the two minima found in the free energy profile (ξ = −2.8 and −6.0 Å, states C and E in Figure 3f) correspond to the bridging of different pairs of adjacent clusters by the terminal -NH_2 groups in TETA, in excellent agreement with our experimental data. The interconversion between these minimum states is only separated by a free energy barrier of 12 kJ mol^{-1}, that is probably the reason for the large crystallographic disorder observed inside the cavities.

Our computational analysis suggests that the infiltration of TETA into the microporous cavities in MUV-10 proceeds by a mechanism that requires a cooperative interplay between the conformational changes in the tetraamine and the reversible reconfiguration of the pore windows through breaking/formation of coordination bonds with the Ca^{2+} sites in the framework. The Supplementary Movie S1 gives a dynamic overview of the translocation and confinement process in the two perspectives used to capture the snapshots illustrated in Figure 3f. This phenomenon is an excellent example of how the dynamic character of carboxylate linkages used in the assembly of multiple porous molecular architectures can lead to structural responses completely inaccessible to more rigid frameworks such as zeolites. In fact, it is the specific combination of soft (Ca^{2+}) and hard (Ti^{+4}) nodes in the Ti_2Ca_2 cluster that appears to be responsible for endowing the pore windows with the ability to adapt their opening to the passage of the infiltrating guest without a significant stability penalty. The combination of rigid Ti–O and dynamic Ca–O bonds, with bond dissociation energies of 662 and 464 kJ mol^{-1},[47] in a 50 % ratio is probably responsible for accommodating significant local structural changes without inducing an irreversible structural collapse. We argue this combination of dynamic and rigid bonds in MUV-10 is also responsible for the ability of this MOF to topologically transform into ***mtn*** and ***tbo*** nets by transmetallation reactions.[48]

Amine Content and Impact on MUV-10-TETA Properties

As previously mentioned, our preliminary analysis of MUV-10-TETA with ^{1}H NMR anticipated an amine content of close to 1 tetraamine per cluster, compared to the 0.75 molecules expected from the crystallographic cell content. Considering the topology of MUV-10 that combines octa- and cuboctahedral cavities of very close sizes of about 1 nm internal diameter, this deviation could indicate the partial presence of additional tetraamine in the cuboctahedral cavities that are integrated into the 3D channel network of the framework and would act as a gateway for further infiltration into the octahedral ones with a much narrower opening and less accessibility (Figure 4a). We decided to improve our washing protocol, that originally involved anhydrous toluene and hexane only, by adding an additional step in the washing procedure and moving to the use of a polar solvent such as non-anhydrous acetone. This acetone washing was effective in reducing the amine content to the 0.75 TETA molecules per cluster, consistent with the exclusive occupancy of octahedral cavities anticipated by the crystallographic analysis of MUV-10-TETA.

These results seem to suggest that the use of polar solvents is necessary to remove unconfined amine although its increasing solubilizing power and presence can result in complete stripping or partial degradation of the framework. To clarify the impact of the washing protocol we made a comparative study of the material prior to grafting (pristine) and after washing with hexane/toluene (nonpolar) and acetone (polar). The SEM analysis confirms that the crystals are insensitive to the polarity of solvent and retain their morphology in all cases (Supplementary Sections S.5.3 and S.5.4). Comparison of the PXRD patterns with the simulated diffraction of MUV-10 also confirms the structural integrity in all cases and only shows small variations in the relative intensity of some of the diffraction peaks, probably associated with relative changes in pore content (Figure 4b). The N_2 adsorption/desorption isotherms at 77 K show a clear decrease of the gas uptake that seems to correlate directly with the net amine content of the material after washing. The experimental pore volume of 0.40 cm^3 g^{-1} in pristine MUV-10 is reduced by near to 40 % in MUV-10-TETA as result of amine incorporation from an initial uptake of 260 to 155 cm^3 g^{-1} after the amine grafting. In addition, the removal of unconfined amine after washing with acetone allows the recovery of 13 % of the original porosity, for an uptake of 190 cm^3 g^{-1} Figure 4c). As confirmed by the pore size distribution plot, these relative variations are all associated with a well-defined pore centered at 1 nm in diameter (Figure 4d). It is worth noting that the use of N_2 as probe does not enable to discriminate between the two

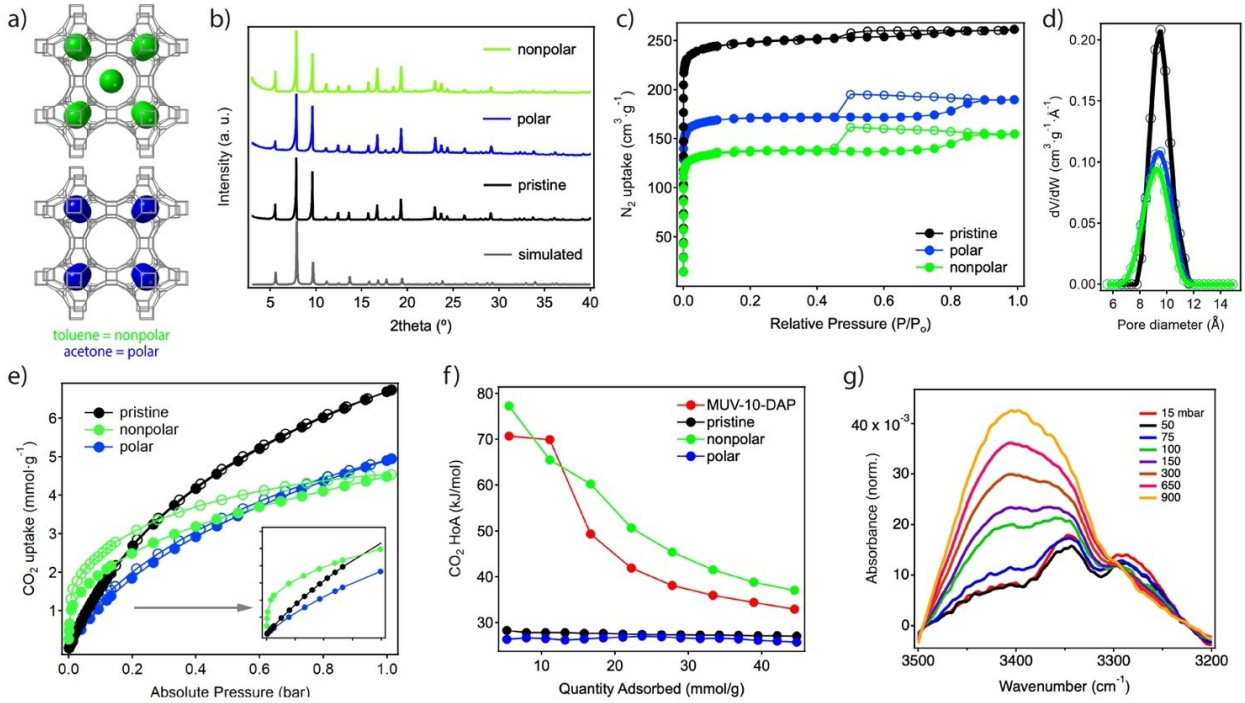

Figure 4. Amine content and impact on MUV-10-TETA properties. a) Possible locations of TETA in the MUV-10 framework after washing with toluene/nonpolar (green) or acetone/polar (blue) solvents. b) Comparison of the simulated and experimental PXRD patterns of MUV-10 and MUV-10-TETA after washings with nonpolar and polar solvents. c) Changes in the experimental uptake of N_2 and d) pore size distribution from N_2 isotherms associated to variations of amine content in the solid. The PSD plot was calculated with nonlinear DFT methods. e) CO_2 adsorption isotherms at 273 K. The inset is a magnification of the low-pressure region showing the change in slope associated to the relative differences in amine content. f) Heat of adsorption of CO_2 calculated from the 273, 283 and 293 K adsorption isotherms by using the Clausius-Clapeyron equation. The presence of unconfined amine in MUV-10-DAP and MUV-10-TETA washed with a nonpolar solvent is responsible for the boost in Q_{st}. g) Baseline corrected *in situ* FT-IR spectra of MUV-10-TETA-nonpolar upon dosing of CO_2 at varying pressures (0–900 mbar).

accessible cavities that overlap into a single signal in the PSD plot.

We next performed CO_2 adsorption experiments. The data collected at 273 K reveal a similar trend in the changes of the uptake at high relative pressures, with a drop of about 25 % in MUV-10-TETA as result of amine incorporation, which is further reduced due to the presence of residual amine in the absence of acetone washing (Figure 4e). Another fact that drew our attention was the differences in slope of these adsorption isotherms at low pressures, indicative of changes in the CO_2-framework interaction. In fact, the presence of residual amine in the channels seems to be responsible for a much more favorable interaction with CO_2 molecules when compared to the lower and almost identical slopes of the other two materials. To confirm this fact, we also measured CO_2 adsorption isotherms at different temperatures to calculate the heat of adsorption (HOA) for CO_2 (Figure 4f). The presence of residual amines in the 3D channels yields a Q_{st} value close to 80 kJ mol^{-1}. This value is close to the highest isosteric heats between 100–75 kJ mol^{-1} described for the grafting of amines and amino acids,[30,49–51] and very close to the 70 kJ mol^{-1} measured under the same conditions for MUV-10-DAP. In both cases, the presence of tetraamine or diamine molecules in the channels seems to offer strong anchoring points for CO_2. On the other hand, the confinement of TETA into the octahedral cavities seems to completely inhibit this behavior by assimilating it to the pristine material for almost identical values of near to 30 kJ mol^{-1}. This behavior suggests a very effective shielding of tetraamine in the cavities of MUV-10, neglecting its interaction with CO_2 as a result not only of the confinement but probably because of the high steric congestion within the cavity, and the restriction to gas diffusion imposed by the narrow pore openings available. As for the adsorption kinetics, TGA analysis indicates that CO_2 diffusion in nonpolar is quite similar to polar or other amine-appended MOFs,[52] discarding the formation of clogged channels as result of the presence of TETA molecules in the channels of the framework (Supplementary Section S.5.10). We also tested the stability of polar and nonpolar against thermal stress under oxidizing conditions[53] to confirm the differences of stability for the different modes of amine grafting (Supplementary Section S.5.11). Fresh batches of both materials were heated at 100 °C under an air flow for 5 h before recollecting CO_2 adsorption isotherms. We observe a clear drop in the slope of the adsorption profile at low-p of nonpolar after the treatment that is indicative of the decomposition of the grafted amine present in the channels under these conditions. In turn, we do not observe significant differences before and after the treatment of polar suggesting that the amines occluded in the cavities do not undergo the same process for almost identical

slopes and negligible interaction with CO_2 that is restrained to physisorption in the amine-free channels. This effect is also evidence by the drastic drop in the HOA of nonpolar down to near 30 kJ mol^{-1} after the treatment whereas the variations registered for polar confirm small changes under this oxidative treatment.

Finally, by using FT-IR spectroscopy of CO adsorption, we studied the effect of the amine grafting in the generation of open metal sites that are accessible in the pristine material by thermal heating in vacuum. As shown in Figure S20, the spectrum of MUV-10-TETA at low CO pressures is dominated by its adsorption to Lewis acid sites (2168 cm^{-1}), while higher pressures also reveal the presence of Brønsted sites (2157 cm^{-1}) accompanied by the CO physisorption band at lower frequencies. This spectrum is practically identical to that of MUV-10,[39] confirming that tetraamine coordination does not inhibit the generation of coordination vacancies. However, the presence of axially coordinated water in 25 % of the Ca^{2+} sites does not allow us to conclude if these vacancies are associated to amine detachment or not. In situ FT-IR experiments at varying CO_2 pressures were also used to confirm chemisorption in MUV-10-TETA-nonpolar.[54] Figure 4g shows the appearance of a vibration centred at 3406 cm^{-1} indicative of carbamate formation that increases its intensity with pressure. The formation of this new band is concomitant to the disappearance of N–H vibrations associated to primary amines at 3345 and 3284 cm^{-1}.

Stability of MUV-10-TETA-Nonpolar under Humid Conditions

One of the main requirements for the application of amine-modified sorbents in post-combustion CO_2 capture processes is their ability to remain stable in the presence of water. The way in which the amine is distributed and coordinated to the sorbent may determine its robustness to stripping or degradation in the presence of water or other polar solvents.[33,36] In this regard, all our results point to the fact that the caging of the tetraamine TETA within the octahedral cavities of MUV-10 results in an enhanced stability against water, that is not observed for the diamine DAP in the same sorbent. The TETA permeates into the less accessible octahedral cavities of MUV-10 for a very tight confinement that might be more effective in avoiding stripping or degradation (Figure 5a). On the other hand, if

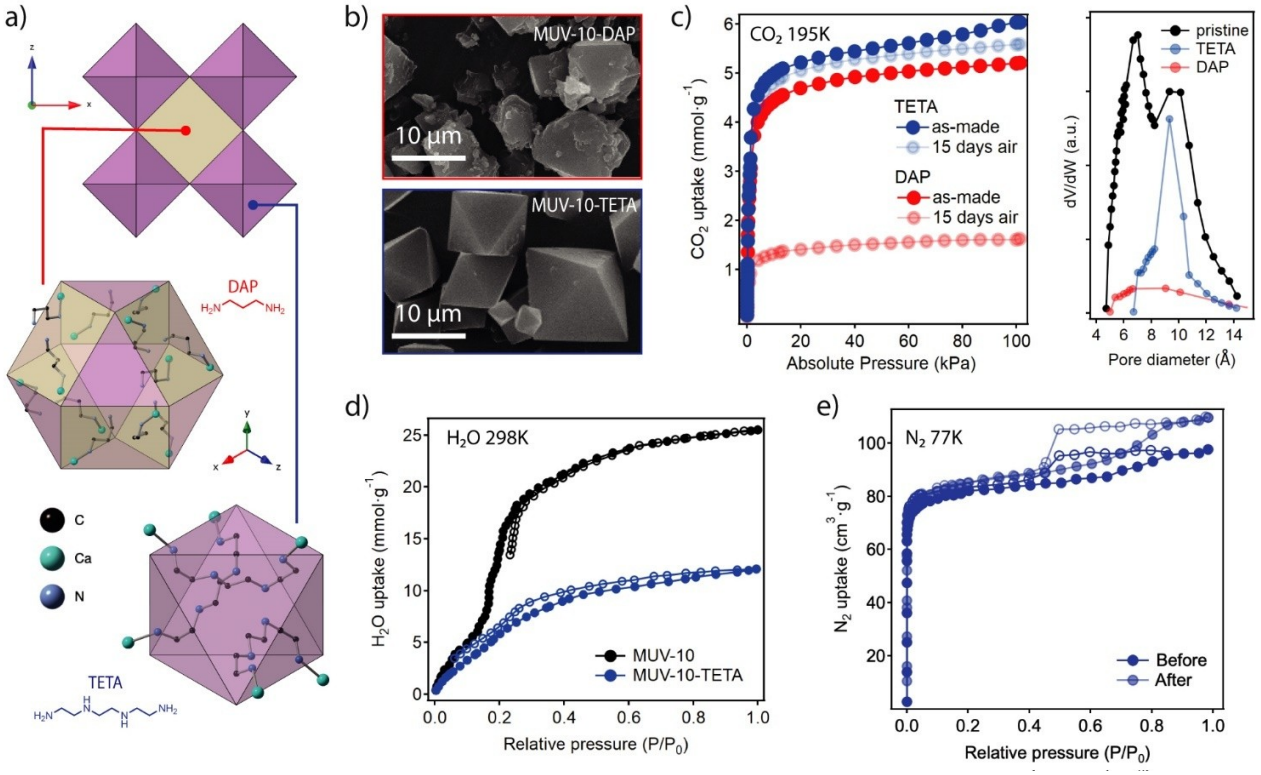

Figure 5. Stability of MUV-10-TETA-nonpolar under humid conditions. a) Underlying connectivity and tessellation in MUV-10 and coordination of DAP and TETA in the corresponding cubooctahedral and octahedral cavities in the framework. b) SEM image showing the changes in the morphology of MUV-10-DAP and TETA crystals after 15 days of exposure to ambient conditions. c) Adsorption isotherm of CO_2 at 195 K of both solids before/after exposure to air confirming the degradation of DAP compared to the retention of porosity in TETA. The inset shows the corresponding PSD plots for all materials after exposure to air confirming the discrimination of accessible cavities imposed by TETA and complete degradation in the DAP case. d) Differences in the water adsorption isotherms at 298 K of MUV-10 before and after TETA encapsulation that confirms the restriction imposed by amines to condensation in the occupied cavities. e) Retention of the N_2 uptake after the water adsorption isotherm, supporting the stability of MUV-10-TETA in presence of water.

considering the same translocation mechanism for the mono-dentate DAP, its smaller molecular size and conformational space may lead to an easier and reversible translocation between the 3D channel and octahedral cage, in comparison to the bi-dentate TETA. Consequently, DAP molecules would be more exposed/susceptible to solvent molecules with high affinity for amine interaction. To account for these differences, we prepared new batches of MUV-10-TETA-nonpolar and DAP, this last according to our reported procedure,[39] and cleaned them with anhydrous toluene and hexane for meaningful comparison. It is worth noting that, under these conditions, the TETA analogue would be expected to include pendant amines in the cuboctahedral cavities more prone to interaction with water. Both solids were left to stand in open air for 1 month. For this period, relative humidity readings in the laboratory oscillated between 45 and 60 %. The PXRD of both samples after sequential exposition times does not reflect significant structural changes that would allow establishing clear differences between them (Supplementary Section S.6). However, Figure 5b shows how MUV-10-TETA crystals remain intact after 15 days of exposure to the environment while the DAP analogue displays damaged crystals that have lost their original morphology. These differences suggest a severe degradation of MUV-10-DAP in the presence of ambient humidity, although it is not visible from diffraction, possibly due to the formation of an amorphous material. To quantitatively evaluate the damage to the framework, we compared the CO_2 adsorption isotherms at 195 K of both materials before and after exposure to humidity (Figure 5c). Compared to MUV-10-TETA that shows small changes, the CO_2 adsorption capacity of DAP is greatly diminished to the extent that it is reduced by about 75 % compared to the as-made material. As for the cavities available, CO_2 can discriminate between the two unlike N_2. After exposure to the environment, both pores can be differentiated in the case of MUV-10. The grafting of TETA restricts CO_2 adsorption exclusively to the cavities in the channels confirming its confinement in the smaller octahedral cavities, while the derivative with DAP completely loses the porosity as result of degradation.

These results reinforce the differences in stability associated with the different location and coordination mode of DAP and TETA. While the former results in a very evident degradation in contact with moisture, probably associated with the stripping of the amine and generation of a very basic medium, the encapsulation of TETA in the octahedral cavities allows it to withstand the same conditions with minimal impact on the structure and porosity of the material. To confirm this stability under even more extreme conditions, we also measured the water adsorption isotherm of MUV-10-TETA (Figure 5d). The isotherm of MUV-10 shows a first adsorption step at low pressures ($p/p_0 < 0.2$), due to the condensation of water at the hydrophilic sites in the channels, followed by the filling of the octahedral cavities at higher pressures up to a maximum uptake of near 0.5 $g\,g^{-1}$ at 298 K. In contrast, the presence of TETA disables the condensation of water in the cavities and restricts the adsorption exclusively to the channels. Although the absence of hysteresis is already indicative of the robustness of MUV-10-TETA under these conditions, Figure 5e confirms that its ability to adsorb N_2 remains almost unchanged compared to that of the same material before being exposed to water.

Conclusion

We introduce an alternative mechanism for the integration of tetraamines in porous frameworks, that is intrinsic to the use of heterobimetallic Ti_2Ca_2 SBUs and adds up to the pool of opportunities offered by heterometallic titanium-oxo clusters to control framework function,[55] now extended to adaptable response for small molecule translocation. The combination of hard and soft coordination sites in the cluster allows MUV-10 crystals to undergo an adaptable response in the presence of triethylenetetramine molecules. The node's flexibility facilitates the translocation of tetraamines into microporous cavities that are difficult to access thanks to the reversible reconfiguration of the pore windows enabled by dynamic Ca–O bonds. Our simulations suggest that the harder Ti^{4+} sites, which remain unchanged, are essential for maintaining structural integrity during the process, and compared to smaller diamines, this grafting mode is specific to TETA and very efficient in protecting the confined, bis-coordinated adducts in humid environments, preventing detachment and framework degradation even after water uptake experiments.

Compared to the well-established grafting by metal vacancy generation and direct amine coordination often used for MOFs and other porous supports, this translocation route is not accessible to rigid coordination bonds and highlight the unique opportunities offered by molecular frameworks in the design of amine-appended sorbents by alternative methods. Although the internal diameter, window apertures, and high steric congestion in the amine rich cavities of MUV-10-TETA prevent potential interactions with CO_2, making it unsuitable for capture applications, we are currently extending this methodology to isoreticular ***the***-MOFs with tailorable cavities from 1.5 to 3 nm,[38] to circumvent this limitation, and demonstrate the opportunities offered by this translocation method in the design of solid adsorbents for decarbonization technologies.[55,38]

Acknowledgements

This work was supported by the H2020 program (ERC-2021-COG-101043428), the Generalitat Valenciana (PROMETEU/2021/054, IDIFEDER/2021/075 and MFA/2022/026) and the Spanish government (CEX2019-000919-M, PID2020-118117RB-I00 and CNS2022-135677). A. R.-G. acknowledges the Generalitat Valenciana for a predoctoral grant (ACIF/2020/090). We also thank the University of Valencia for research facilities (NANBIOSIS). S.N. thanks the support of grant PID2021-123856OBI00 funded by MICIU/AEI/10.13039/501100011033 and by ERDF A way of making Europe. We also thank ALBA (XALOC BL13,

2022086946) and Diamond Light Source (I-19, CY28808-1) for the access to Synchrotron beamtime. BSC-RES is also acknowledged for computational resources (QHS-2023-2-0016 and QHS-2023-3-0022).

Conflict of Interest

The authors declare no conflict of interests.

Data Availability Statement

The data that support the findings of this study are available from the corresponding author upon reasonable request.

Keywords: tetraamine · translocation · confinement · cluster chemistry · pore reconfiguration · nanoporous cavities

[1] H. Furukawa, K. E. Cordova, M. O'Keeffe, O. M. Yaghi, *Science* **2013**, *341*, 1230444.
[2] C. S. Diercks, O. M. Yaghi, *Science* **2017**, *355*, eaal1585.
[3] O. M. Yaghi, *ACS Cent. Sci.* **2019**, *5*, 1295–1300.
[4] Z. Ji, H. Wang, S. Canossa, S. Wuttke, O. M. Yaghi, *Adv. Funct. Mater.* **2020**, 2000238.
[5] H. Furukawa, N. Ko, Y. B. Go, N. Aratani, S. B. Choi, E. Choi, A. O. Yazaydin, R. Q. Snurr, M. O'Keeffe, J. Kim, O. M. Yaghi, *Science* **2010**, *329*, 424–428.
[6] J. A. Mason, J. Oktawiec, M. K. Taylor, M. R. Hudson, J. Rodriguez, J. E. Bachman, M. I. Gonzalez, A. Cervellino, A. Guagliardi, C. M. Brown, P. L. Llewellyn, N. Masciocchi, J. R. Long, *Nature* **2015**, *527*, 357–361.
[7] Z. Chen, P. Li, R. Anderson, X. Wang, X. Zhang, L. Robison, L. R. Redfern, S. Moribe, T. Islamoglu, D. A. Gómez-Gualdrón, T. Yildirim, J. F. Stoddart, O. K. Farha, *Science* **2020**, *368*, 297–303.
[8] X. Han, S. Yang, M. Schröder, *J. Am. Chem. Soc.* **2023**, *145*, 1998–2012.
[9] X.-P. Yan, M. J. Zaworotko, *Chem* **2017**, *3*, 281–289.
[10] J. Navarro-Sánchez, A. I. Argente-García, Y. Moliner-Martínez, D. Roca-Sanjuán, D. Antypov, P. Campíns-Falcó, M. J. Rosseinsky, C. Martí-Gastaldo, *J. Am. Chem. Soc.* **2017**, *139*, 4294–4297.
[11] L. Li, R.-B. Lin, R. Krishna, H. Li, S. Xiang, H. Wu, J. Li, W. Zhou, B. Chen, *Science* **2018**, *362*, 443–446.
[12] S. Zhou, O. Shekhah, J. Jia, J. Czaban-Jóźwiak, P. M. Bhatt, A. Ramírez, J. Gascon, M. Eddaoudi, *Nat. Energy* **2021**, *6*, 882–891.
[13] Y. Su, K. Otake, J.-J. Zheng, S. Horike, S. Kitagawa, C. Gu, *Nature* **2022**, *611*, 289–294.
[14] H. Wang, Q.-L. Zhu, R. Zou, Q. Xu, *Chem* **2017**, *2*, 52–80.
[15] Y.-S. Wei, M. Zhang, R. Zou, Q. Xu, *Chem. Rev.* **2020**, *120*, 12089–12174.
[16] A. Bavykina, N. Kolobov, I. S. Khan, J. A. Bau, A. Ramirez, J. Gascon, *Chem. Rev.* **2020**, *120*, 8468–8535.
[17] A. Iliescu, J. J. Oppenheim, C. Sun, M. Dincă, *Chem. Rev.* **2023**, *123*, 6197–6232.
[18] M. Kalaj, S. M. Cohen, *ACS Cent. Sci.* **2020**, *6*, 1046–1057.
[19] S. Lee, E. A. Kapustin, O. M. Yaghi, *Science* **2016**, *353*, 808–811.
[20] A. E. Platero-Prats, A. B. League, V. Bernales, J. Ye, L. C. Gallington, A. Vjunov, N. M. Schweitzer, Z. Li, J. Zheng, B. L. Mehdi, A. J. Stevens, A. Dohnalkova, M. Balasubramanian, O. K. Farha, J. T. Hupp, N. D. Browning, J. L. Fulton, D. M. Camaioni, J. A. Lercher, D. G. Truhlar, L. Gagliardi, C. J. Cramer, K. W. Chapman, *J. Am. Chem. Soc.* **2017**, *139*, 10410–10418.
[21] F. R. Fortea-Pérez, M. Mon, J. Ferrando-Soria, M. Boronat, A. Leyva-Pérez, A. Corma, J. M. Herrera, D. Osadchii, J. Gascon, D. Armentano, E. Pardo, *Nat. Mater.* **2017**, *16*, 760–766.
[22] T. M. McDonald, W. R. Lee, J. A. Mason, B. M. Wiers, C. S. Hong, J. R. Long, *J. Am. Chem. Soc.* **2012**, *134*, 7056–7065.
[23] P. J. Milner, R. L. Siegelman, A. C. Forse, M. I. Gonzalez, T. Runčevski, J. D. Martell, J. A. Reimer, J. R. Long, *J. Am. Chem. Soc.* **2017**, *139*, 13541–13553.
[24] R. W. Flaig, T. M. O. Popp, A. M. Fracaroli, E. A. Kapustin, M. J. Kalmutzki, R. M. Altamimi, F. Fathieh, J. A. Reimer, O. M. Yaghi, *J. Am. Chem. Soc.* **2017**, *139*, 12125–12128.
[25] X. Zhu, W. Xie, J. Wu, Y. Miao, C. Xiang, C. Chen, B. Ge, Z. Gan, F. Yang, M. Zhang, D. O'Hare, J. Li, T. Ge, R. Wang, *Chem. Soc. Rev.* **2022**, *51*, 6574–6651.
[26] M. Ozkan, A.-A. Akhavi, W. C. Coley, R. Shang, Y. Ma, *Chem* **2022**, *8*, 141–173.
[27] Y. K. Hwang, D. Hong, J. Chang, S. H. Jhung, Y. Seo, J. Kim, A. Vimont, M. Daturi, C. Serre, G. Férey, *Angew. Chem. Int. Ed.* **2008**, *47*, 4144–4148.
[28] J. D. Martell, L. B. Porter-Zasada, A. C. Forse, R. L. Siegelman, M. I. Gonzalez, J. Oktawiec, T. Runčevski, J. Xu, M. Srebro-Hooper, P. J. Milner, K. A. Colwell, J. Autschbach, J. A. Reimer, J. R. Long, *J. Am. Chem. Soc.* **2017**, *139*, 16000–16012.
[29] J.-H. Lee, R. L. Siegelman, L. Maserati, T. Rangel, B. A. Helms, J. R. Long, J. B. Neaton, *Chem. Sci.* **2018**, *9*, 5197–5206.
[30] E. J. Kim, R. L. Siegelman, H. Z. H. Jiang, A. C. Forse, J.-H. Lee, J. D. Martell, P. J. Milner, J. M. Falkowski, J. B. Neaton, J. A. Reimer, S. C. Weston, J. R. Long, *Science* **2020**, *369*, 392–396.
[31] M. K. Sarango-Ramírez, D.-W. Lim, D. I. Kolokolov, A. E. Khudozhitkov, A. G. Stepanov, H. Kitagawa, *J. Am. Chem. Soc.* **2020**, *142*, 6861–6865.
[32] M. K. Sarango-Ramírez, J. Park, J. Kim, Y. Yoshida, D. Lim, H. Kitagawa, *Angew. Chem. Int. Ed.* **2021**, *60*, 20173–20177.
[33] S. T. Parker, A. Smith, A. C. Forse, W.-C. Liao, F. Brown-Altvater, R. L. Siegelman, E. J. Kim, N. A. Zill, W. Zhang, J. B. Neaton, J. A. Reimer, J. R. Long, *J. Am. Chem. Soc.* **2022**, *144*, 19849–19860.
[34] J. H. Choe, H. Kim, M. Kang, H. Yun, S. Y. Kim, S. M. Lee, C. S. Hong, *J. Am. Chem. Soc.* **2022**, *144*, 10309–10319.
[35] P. D. C. Dietzel, R. E. Johnsen, H. Fjellvåg, S. Bordiga, E. Groppo, S. Chavan, R. Blom, *Chem. Commun.* **2008**, 5125–5127.
[36] G. Rim, P. Priyadarshini, M. Song, Y. Wang, A. Bai, M. J. Realff, R. P. Lively, C. W. Jones, *J. Am. Chem. Soc.* **2023**, *145*, 7190–7204.
[37] J. Castells-Gil, N. M. Padial, N. Almora-Barrios, J. Albero, A. R. Ruiz-Salvador, J. González-Platas, H. García, C. Martí-Gastaldo, *Angew. Chem. Int. Ed.* **2018**, *57*, 8453–8457.
[38] N. M. Padial, C. Chinchilla-Garzón, N. Almora-Barrios, J. Castells-Gil, J. González-Platas, S. Tatay, C. Martí-Gastaldo, *J. Am. Chem. Soc.* **2023**, *145*, 21397–21407.
[39] E. López-Maya, N. M. Padial, J. Castells-Gil, C. R. Ganivet, A. Rubio-Gaspar, F. G. Cirujano, N. Almora-Barrios, S. Tatay, S. Navalón, C. Martí-Gastaldo, *Angew. Chem. Int. Ed.* **2021**, *60*, 11868–11873.
[40] A. B. Cairns, A. L. Goodwin, *Chem. Soc. Rev.* **2013**, *42*, 4881–4893.
[41] W. You, Z. Tang, C. A. Chang, *J. Chem. Theory Comput.* **2019**, *15*, 2433–2443.

[42] P. Cnudde, R. Demuynck, S. Vandenbrande, M. Waroquier, G. Sastre, V. V. Speybroeck, *J. Am. Chem. Soc.* **2020**, *142*, 6007–6017.
[43] P. Cnudde, E. A. Redekop, W. Dai, N. G. Porcaro, M. Waroquier, S. Bordiga, M. Hunger, L. Li, U. Olsbye, V. V. Speybroeck, *Angew. Chem. Int. Ed.* **2021**, *60*, 10016–10022.
[44] R. Millan, P. Cnudde, V. van Speybroeck, M. Boronat, *JACS Au* **2021**, *1*, 1778–1787.
[45] K. Fabrizio, K. A. Lazarou, L. I. Payne, L. P. Twight, S. Golledge, C. H. Hendon, C. K. Brozek, *J. Am. Chem. Soc.* **2021**, *143*, 12609–12621.
[46] E. S. Grape, A. M. Davenport, C. K. Brozek, *Dalton Trans.* **2024**, *53*, 1935–1941.
[47] J. Dean, *Lange's Handbook of Chemistry*, McGraw-Hill Inc., Madrid, **1990**.
[48] N. M. Padial, B. Lerma-Berlanga, N. Almora-Barrios, J. Castells-Gil, I. da Silva, M. de la Mata, S. I. Molina, J. Hernández-Saz, A. E. Platero-Prats, S. Tatay, C. Martí-Gastaldo, *J. Am. Chem. Soc.* **2020**, *142*, 6638–6648.
[49] A. Demessence, D. M. D'Alessandro, M.-L. Foo, J. R. Long, *J. Am. Chem. Soc.* **2009**, *131*, 8784–8786.
[50] T. M. McDonald, J. A. Mason, X. Kong, E. D. Bloch, D. Gygi, A. Dani, V. Crocellà, F. Giordanino, S. O. Odoh, W. S. Drisdell, B. Vlaisavljevich, A. L. Dzubak, R. Poloni, S. K. Schnell, N. Planas, K. Lee, T. Pascal, L. F. Wan, D. Prendergast, J. B. Neaton, B. Smit, J. B. Kortright, L. Gagliardi, S. Bordiga, J. A. Reimer, J. R. Long, *Nature* **2015**, *519*, 303–308.
[51] H. Lyu, O. I.-F. Chen, N. Hanikel, M. I. Hossain, R. W. Flaig, X. Pei, A. Amin, M. D. Doherty, R. K. Impastato, T. G. Glover, D. R. Moore, O. M. Yaghi, *J. Am. Chem. Soc.* **2022**, *144*, 2387–2396.
[52] J. D. Martell, P. J. Milner, R. L. Siegelman, J. R. Long, *Chem. Sci.* **2020**, *11*, 6457–6471.
[53] P. Bollini, S. Choi, J. H. Drese, C. W. Jones, *Energy Fuels* **2011**, *25*, 2416–2425.
[54] Z. Zhu, H. Tsai, S. T. Parker, J.-H. Lee, Y. Yabuuchi, H. Z. H. Jiang, Y. Wang, S. Xiong, A. C. Forse, B. Dinakar, A. Huang, C. Dun, P. J. Milner, A. Smith, P. G. Martins, K. R. Meihaus, J. J. Urban, J. A. Reimer, J. B. Neaton, J. R. Long, *J. Am. Chem. Soc.* **2024**, *146*, 6072–6083.
[55] J. Castells-Gil, N. Almora-Barrios, B. Lerma-Berlanga, N. M. Padial, C. Martí-Gastaldo, *Chem. Sci.* **2023**, *14*, 6826–6840.

Manuscript received: February 9, 2024
Accepted manuscript online: April 21, 2024
Version of record online: May 28, 2024